Pergamon

Int. J. Heat Mass Transfer. Vol. 39, No. 9, pp. 1953–1961, 1996

0017–9310/96 $15.00+0.00

0017–9310(95)00267–7

Transient heat transfer from surfaces of defined roughness into liquid nitrogen

V. DRACH, N. SACK and J. FRICKE†

Bavarian Centre for Applied Energy Research (ZAE Bayern) and Physics Department of the University, Am Hubland, D-97074 Würzburg, Germany

(*Received* 17 *November* 1994 *and in final form* 20 *June* 1995)

Abstract—This paper presents experiments which quantify the influence of the surface roughness on transient heat transfer from a substrate into liquid nitrogen. Using vapor-deposited metal films on glass substrates of different roughness the temperature variation of a surface subjected to a heat pulse was recorded. In addition optical methods were used to observe bubble formation and growth. Onset of nucleate boiling, temperature development and critical heat flux are investigated and compared with theoretical predictions. It is shown that for rough surfaces the onset of nucleate boiling occurs at lower temperatures and thus after smaller delay than for smooth surfaces. Furthermore, rough surfaces exhibit higher critical transient heat fluxes characterizing the transition to film boiling. The interpretation of photographs suggests that evaporation of liquid into one big vapor bubble dominates the transient heat transfer after onset of nucleate boiling.

1. INTRODUCTION

Liquid nitrogen (LN_2) is a cheap, efficient and non-corrosive coolant. One of its cryogenic applications is the cooling of integrated electronic circuits in order to enable higher processing speeds and higher power densities. Since the discovery of ceramic HT_c- superconductors LN_2 has become even more important, because its boiling temperature of 77.4 K (at atmospheric pressure) is lower than the critical temperature of many HT_c- superconductors. This promises operation of superconducting components without the use of liquid helium as an expensive coolant. Superconducting magnetic energy storage (SMES), power transmission lines or fast current switches are examples for possible applications in power industry [1, 2]. In designing these high-current components questions of thermal stability play an important role [3, 4]. Local disturbances like wire movements or flux jumps can produce resistive and thus heat-generating regions in the superconductor. These 'hot spots' may spread and cause quenching of the whole system. The temperature history of the system and the development of a quench will depend substantially upon the efficiency with which heat is transferred to the coolant. This process is transient, which has to be taken into account when examining thermal stability of the superconducting component.

Experiments on transient heat transfer into liquid helium [5, 6] provided useful information for the design of conventional superconducting magnets. Investigations concerning liquid nitrogen as a coolant have been carried out by several researchers using a wire as heat source [7–9]. In addition Oker and Merte [10] and Giarratano [11] presented results for a plane-heater on a smooth glass substrate. These investigations [5–11] revealed that results derived from stationary experiments (e.g. [12]) cannot be directly applied to transient experiments. The reason is the time lag in the onset of nucleate boiling and convection, which (besides heat conduction and radiation) are the main mechanisms in transferring heat from a surface into a liquid. On the other hand it is known from stationary experiments, that surface shape and roughness are of great importance for bubble nucleation and therefore for the heat transfer (see e.g. [13–15]). To the authors' knowledge this effect has not been examined in transient experiments yet. Therefore this paper focusses on the influence of surface roughness on the transient heat transfer. This is of particular interest for applications where the ceramic surface of a HT_c- superconductor contacts the coolant LN_2 directly. Furthermore, the paper shows how to optimize the transient heat transfer via surface treatment and gives quantitative results for the improvement.

2. EXPERIMENTAL TECHNIQUE

Similar to measurements of other investigators [10, 11] we applied a hot-strip-technique: a metal film vapor-deposited on the substrate to be investigated, serves both as heater and temperature sensor. Thus there is no lag between thermal excitation and response and transient thermal processes at the submerged surface can be resolved. Another advantage is the negligible thermal influence of the metal strip on the thermal behavior of the substrate because of the

† Author to whom correspondence should be addressed.

NOMENCLATURE

A	heater/thermometer area [cm^2]
C	constant in Kutateladze's equation
c_p	specific heat capacity [$J\ kg^{-1}\ K^{-1}$]
Δh	specific heat of vaporisation [$J\ kg^{-1}$]
I	current [A]
J	nucleation rate [$cm^{-3}\ s^{-1}$]
k	Boltzmann constant $= 1.38054 \times 10^{-23}\ J\ K^{-1}$
m	mass of one molecule [kg]
N	liquid particle density [cm^{-3}]
P	power [W]
p	pressure [Pa]
Q	accumulated heat [J]
$\dot{q}$	power per unit area; heat flux [$W\ cm^{-2}$]
R	resistance [Ω]
ΔR	resistance increase [Ω]
R_a	mean roughness [μm]
R_t	peak roughness [μm]
r	bubble radius [m]
T	temperature [K]
ΔT	temperature increase [K]
t	time [s]
ΔU	voltage at bridge [V]
V	vapor volume [cm^{-3}].

Greek symbols

α	temperature coefficient [$\Omega\ K^{-1}$]
ε	thermal effusivity [$W\sqrt{s}\,K^{-1}\ m^{-2}$]
λ	thermal conductivity [$W\ m^{-1}\ K^{-1}$]
ρ	density [$kg\ m^{-3}$]
σ	surface tension [$N\ m^{-1}$].

Subscripts

cr	critical
kl	kinetic limit
l	liquid
max	maximal
b	onset of nucleate boiling
s	substrate, specimen
sat	saturation
st	standard
tl	thermodynamic limit
v	vapor
0	initial.

small thickness and heat capacity of the strip. On the other hand heat transferred into the substrate must be taken into account.

Figure 1 illustrates the experimental setup schematically. Heat is generated in the metal strip by applying a constant-current pulse (I) of variable duration and strength to sensor (R_0) and standard resistor (R_{st}). The temperature increase during the current pulse is detected via the increase of the voltage drop across the metal strip with its known temperature-dependent resistivity. The resistance increase due to the temperature rise is denoted ΔR; R_0 is the sensor resistance at the starting temperature (here 77.4 K). In order to isolate the voltage due to resistance increase from the constant shift ($I \cdot R_b$), we used a Thompson double-bridge. Its resistances (R_1, R_2) being in the range of 10 kΩ are large compared to the sensor and standard resistances, which are in the range of 1 Ω. Assuming the bridge to be balanced ($R_1/R_2 = R_0/R_{st}$) its output is

$$\Delta U = \frac{R_{st}}{R_{st} + R_0} \cdot I \cdot \Delta R. \tag{1}$$

This signal is amplified tenfold and recorded via the analog-to-digital-converter of a multifunction-board or a digital storage oscilloscope. Caused by the temperature–resistance increase during each measurement cycle the electrically deposited power $P = R \cdot I^2$ is not constant, but shows a small variation (less than 4% for all experiments performed in this work). Stated values of the electrically deposited thermal power density $\dot{q} = P/A$ are always averaged over the measurement duration.

Heat transfer measurements were carried out at atmospheric pressure in a reflection-coated LN_2-cryostat with two windows on opposite sides for visual observation. Thus a He–Ne laser beam passing over the heated surface could be used to record the onset of bubble formation. Its intensity was detected by a photo diode positioned on the axis of the beam. Additionally photographs with a computer-triggered flash-lamp were taken. Growth of bubbles could be recorded by repeating the heat transfer experiment under variation of the time delay for the exposure.

To compute the surface-temperature increase ΔT from the resistance shift ΔR in equation (1), the temperature coefficient $\alpha = dR/dT$ of the metal strip had to be known. Therefore measurements of resistance versus temperature were carried out for each specimen in a vacuum chamber immersed in liquid nitrogen. By controlled heating of the specimen its resistance versus temperature dependence was obtained in the temperature range between 79 K and 300 K. All described heat transfer experiments were carried out with the heated surface oriented horizontally and facing upwards.

3. THEORETICAL BACKGROUND

In the following we do not consider radiation and convection for different reasons. At low temperatures the heat transferred by radiation is small compared to

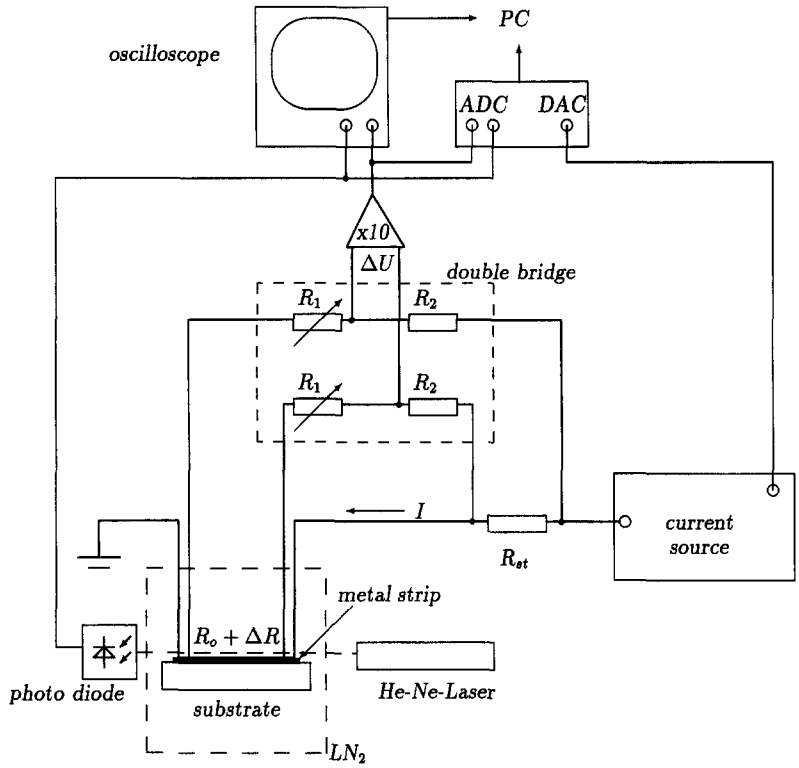

Fig. 1. Schematic diagram of experimental setup. The adjustable resistances (R_1) of the bridge are mechanically coupled.

the heat transferred by conduction and evaporation, due to the T^4-dependence of the Stefan–Boltzmann radiation law. Therefore it may be neglected in the described LN_2-experiments. Convection was found not to be important on the time scale examined in our transient experiments (see Sections 5.2 and 5.4). However, it is implicated in the estimation of stationary critical heat flux by Kutateladze's relation [equation (8)].

3.1 *Heat conduction*

If heat conduction is the only heat transfer mechanism the temperature change in a plane geometry can be evaluated by solving the one-dimensional equation of heat conduction [16]. With a constant power per unit area $\dot{q}$ deposited at the specimen surface for times $t > 0$ and thermal properties being constant, heat conduction into a semi-infinite medium leads to an increase of the surface temperature

$$\Delta T(t) = T - T_0 = \frac{2 \cdot \dot{q}}{\sqrt{\pi} \cdot \varepsilon} \cdot \sqrt{t}. \tag{2}$$

Here $\varepsilon = \sqrt{(\lambda \rho c_p)}$ is the thermal effusivity ε_s of the (thermally insulated, semi-infinite) specimen. Following the derivation of equation (2) it can be shown that in the presence of an adjacent liquid, i.e. when the system is finite instead of semi-infinite, $\varepsilon = \varepsilon_s + \varepsilon_l$ is the sum of the effusivities of specimen and liquid. In this case the total electrically generated power per unit area $\dot{q}$ splits up into substrate ($\dot{q}_s$) and liquid ($\dot{q}_l$) according to the ratio of their effusivities

$$\frac{\dot{q}_s}{\dot{q}_l} = \frac{\varepsilon_s}{\varepsilon_l} \quad \text{with} \quad \dot{q} = \dot{q}_s + \dot{q}_l. \tag{3}$$

3.2 *Onset of nucleate boiling*

Since the starting temperature in the experiment is the boiling point of liquid nitrogen, heat conduction into the adjacent fluid will cause superheating. This condition is not stable and the nucleation of bubbles will start. In order to form a bubble of radius r within the liquid a superheating of [18]

$$\Delta T = T - T_{sat} = \frac{2 \cdot \sigma \cdot T_{sat}}{\Delta h \cdot \rho_v} \cdot \frac{1}{r} \tag{4}$$

is required. Equation (4) resolved for r defines the size of a bubble that is metastable within the liquid superheated by ΔT. Bubbles smaller than this value of r will collapse, greater ones can grow and initiate nucleate boiling.

According to equation (4) the formation of a bubble starting with size $r = 0$ would require infinite superheating. A rough estimation of the maximum temperature attainable without bubble nucleation is obtained from thermodynamic stability criteria [17, 18]. On the base of the van-der-Waals equation of state, regimes of stable, metastable and unstable liquid

can be distinguished. The latter violates the condition $(\partial p/\partial V)_r < 0$, which is necessary for stability. Thus the thermodynamic maximum in superheating ΔT_{tl}, sometimes denoted the liquid spinodal, is obtained by setting $(\partial p/\partial V)_r = 0$. Carey [18] found for liquid nitrogen at atmospheric pressure

$$\Delta T_{tl} = 29.7 \text{ K corresponding to } T_{tl} = 107.1 \text{ K}. \tag{5}$$

The limit of superheating due to internal fluctuations is described by classical theory of nucleation considering the kinetics of bubble formation processes (summarized in [17, 18]). In the case of homogeneous nucleation within the liquid the rate of bubble formation per unit time per unit volume is [17]

$$J = N \cdot \sqrt{\left(\frac{3\sigma}{\pi m}\right)} \cdot \exp\left[\frac{-16\pi\sigma^3}{3kT(p_{sat}-p_l)^2\delta^2}\right]$$

with

$$\delta = 1 - \frac{\rho_v}{\rho_l} + \frac{1}{2}\left(\frac{\rho_v}{\rho_l}\right)^2. \tag{6}$$

Due to the dominating exponential term in equation (6) and the temperature dependence of σ and p_{sat} the rate of bubble formation exhibits an increase of many orders of magnitude with the increase in temperature. It was experimentally found [17], that nucleation happens if a rate of $J \approx 10^5$ cm^{-3} s^{-1} is reached. Using thermophysical properties of liquid nitrogen [19] and $p_l = 1013$ mbar the kinetic limit of superheating ΔT_{kl} is obtained for

$$\Delta T_{kl} = 32.8 \text{ K} \quad \text{corresponding to} \quad T_{kl} = 110.2 \text{ K}. \tag{7}$$

3.3 *Critical heat flux*

Temperature history and heat transfer after onset of nucleate boiling is the result of a complex combination of heat conduction, convection and evaporation. Formation of numerous bubbles and extensive vapour generation may cause film boiling by coalescence of adjacent bubbles also at transient conditions. Kutateladze's relation [20], based on dimensional analysis, predicts the value of the critical heat flux ($\dot{q}_{cr}$). It characterizes the transition from nucleate boiling to film boiling under stationary conditions:

$$\dot{q}_{cr} = C \cdot \rho_v \Delta h \cdot \left[\frac{\sigma(\rho_l - \rho_v)g}{\rho_v^2}\right]^{1/4}. \tag{8}$$

The empirical constant C is estimated to be in the range between 0.131 and 0.149 [18]. Setting $C = 0.135$ [21], a value of $\dot{q}_{cr} \approx 16$ W cm^{-2} is obtained for the critical heat flux of liquid nitrogen at atmospheric pressure.

4. SAMPLES AND PREPARATION

Glass was chosen as model substrate for several reasons. Since it is electrically insulating, preparation of an electrically heated hot-strip on its surface is possible without the need for an insulating interlayer. Furthermore, it has a low temperature-expansion coefficient. Its moderate effusivity guarantees that a sufficient portion of the heat generated at the surface is transferred into the adjacent fluid. Untreated glass possesses an extraordinarily smooth surface, which can be easily roughened by sandblasting.

The samples were microscope slides of soda-lime-glass (Menzel Glasbearbeitungswerk, Germany), which were available with untreated and frosted surfaces. To vary the surface roughness systematically, sandblasting with different pressure and distance was performed. Roughness was characterized using a scanning profilometer with a needle radius of about 1 μm. The values of mean roughness (R_a) and maximum roughness (R_t) for a reference length of 2.5 mm serve as an integral measure for the surface roughness of the investigated samples and are summarized in Table 1. It has to be kept in mind, that the lateral resolution of this technique is limited by the finite needle radius to about 1 μm and narrower grooves were not detected with the profilometer. Extensions of this technique in order to determine cavity-size distributions are used e.g. in [15].

The substrate was cleaned ultrasonically in soda lye, distilled water and acetone. Because of its high temperature coefficient nickel was used for the heater/thermometer strip. The vapor-deposition was carried out via electron-gun evaporation using a mask to define the width of the strip to 10 mm. Additionally deposited silver contact pads define the heater length (22 mm). Because of its small thickness of about 80 nm the metal film does not affect the surface roughness. This was observed with an optical microscope and with measurements of the surface roughness beside and upon the metal film.

5. RESULTS AND DISCUSSION

5.1. *Apparatus performance*

Fused silica "Synsil" (Westdeutsche Quarzschmelze, Germany) was used to test the apparatus.

Table 1. Roughness of investigated specimens as determined by a scanning profilometer. R_a and R_t are evaluated according to DIN 4762

R_a [μm]	R_t [μm]	Procedure
<0.1	<0.1	Untreated
1.4	8.2	Frosted (sandblasted)
2.0	15	Sandblasted
2.4	16	Sandblasted
2.6	19	Sandblasted
3.6	30	Sandblasted
4.8	31	Sandblasted

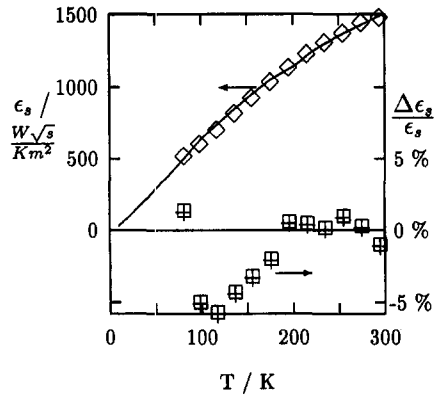

Fig. 2. Measured effusivity ε_s of fused silica (◇) in comparison with literature values (——) [21], [22]. The relative deviations from the literature values are plotted explicitly in the lower part.

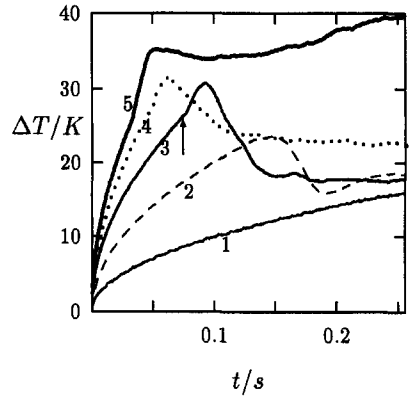

Fig. 4. Measured temperature increase of a smooth surface ($R_a < 0.1$ μm) as a function of time during the heat pulse; (1) $\dot{q} = 2.5$ W cm^{-2}, (2) 5.0 W cm^{-2}, (3) 7.5 W cm^{-2}, (4) 10.0 W cm^{-2}, (5) 11.5 W cm^{-2}. The dash marks the onset of bubble formation exemplary.

Its effusivity (ε_s) was determined according to equation (2) from measurements in a vacuum chamber. The results obtained in the temperature range between 80 K and 300 K are shown in Fig. 2. For comparison values taken from literature [22, 23] are also shown. The maximum error of 6% in our data is mainly due to the error in the determination of the temperature coefficient α.

The error of the temperature detection for the heat-transfer experiments is also dominated by the error in α, which can be estimated by comparing the temperature development of different specimens in the heat conduction regime (cf. Fig. 5). Since the specimens differing in surface roughness possess identical thermal properties, the temperature rise is expected to be identical in the heat conduction regime. Thus an estimated error of 4% was obtained for the determination of the surface temperature.

5.2. *Temperature variation and critical heat flux*

The variation of the surface temperature with time after the heat pulse is switched on is shown in Figs 3

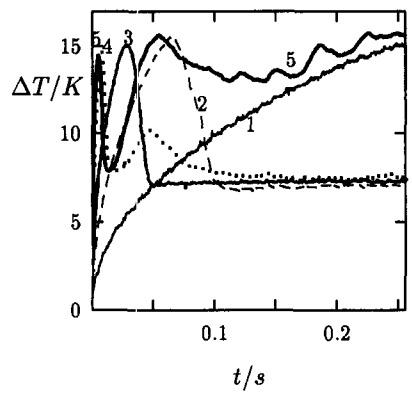

Fig. 3. Measured temperature increase of a rough surface ($R_a = 4.8$ μm) as a function of time during the heat pulse; (1) $\dot{q} = 2.5$ W cm^{-2}, (2) 5.0 W cm^{-2}, (3) 7.5 W cm^{-2}, (4) 15.0 W cm^{-2}, (5) 17.0 W cm^{-2}.

and 4 with the mean dissipated power density $\dot{q}$ as a parameter. Three regimes can be recognized: in the early stages heat conduction is the only heat-transfer mechanism and the temperature increases monotonously. This is valid for the curve no. 1 in Figs 3 and 4 during the whole measurement time. For the other curves (nos 2–5) nucleate boiling starts when a certain degree of superheating is reached. As a result of heat consumed by evaporation of the superheated liquid the surface temperature then decreases and finally approaches a constant value in the regime of nucleate boiling, provided the power input is low (curves no. 2 and no. 3 with $\dot{q} < 14$ W cm^{-2} for a rough and curve no. 2 with $\dot{q} < 7$ W cm^{-2} for a smooth surface). In the case of medium power densities an additional temperature peak is observed. This peak occurs for the rough surface ($R_a = 4.8$ μm) after passing a relative temperature minimum (see curve no. 4 in Fig. 3) and for the smooth surface ($R_a < 0.1$ μm) immediately after the onset of nucleate boiling (see dash in curve no. 3 of Fig. 4). This transient phenomenon can be explained by preliminary formation of an unstable vapor film arising from rapid vapor generation after onset of nucleate boiling. Liquid motion thus tends to disrupt the continuous vapor film. In the case of moderate heat fluxes this leads to stable nucleate boiling. For higher heat fluxes the transition to stable film boiling occurs and the surface temperature increases continuously (see curve no. 5). Here the critical heat flux, which characterizes the transition to film boiling, is surpassed. Stationary values of film boiling would be obtained with longer measurement times. However, our samples were mostly destroyed due to thermal stresses before reaching stationary conditions.

Figure 5 compares the temperature increase with time for different surface roughnesses. In the early stages of heating the temperature variation with time obeys equation (2) and the heat transfer is therefore determined by pure conduction. Convection can be

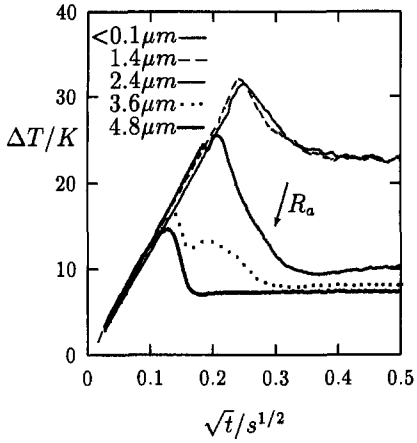

Fig. 5. Temperature increase as a function of $t^{1/2}$ for runs with identical applied power density ($\dot{q}$ = 10 W cm^{-2}) for different surface roughness R_a.

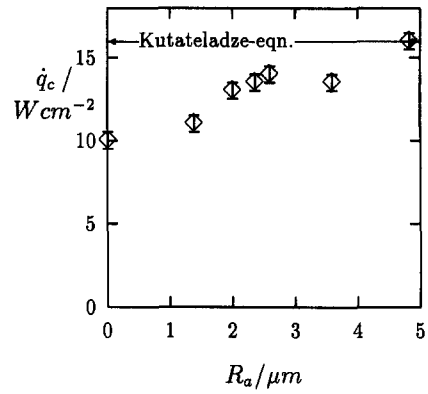

Fig. 6. Measured transient critical heat flux as a function of mean roughness R_a. For comparison the estimated value of Kutateladze's equation (8) for stationary conditions is inserted.

excluded on this time scale. Deviations from square-root behavior are explained by onset of nucleate boiling (see next section). The quasi-stationary temperature shift at the end of the measurement time varies with roughness. This confirms the well-known fact, that the heat transfer coefficient ($\dot{q}/\Delta T$) can be enlarged by increasing the surface roughness (see e.g. [13–15]). The maximum temperature (ΔT_{max}) during the measurement time, which is reached after the onset of boiling, also depends on the surface roughness. ΔT_{max} is a factor of 2 lower for the roughest, sand-blasted surface than for a smooth, untreated surface. Thus the transient excess temperature ΔT_{max} shows a similar dependence on the surface roughness as the corresponding quasi-stationary excess temperature at the end of the measurement time.

The transient critical heat flux ($\dot{q}_{cr}$) was determined by increasing the power input in steps of 0.5 W cm^{-2}. If the excess temperature does not settle to a (quasi-) stationary value after having reached its maximum, the critical heat flux $\dot{q}_{cr}$ has been surpassed, see e.g. curve no. 5 with $\dot{q} > \dot{q}_{cr}$ in Fig. 4, while for curve no. 4 $\dot{q} < \dot{q}_{cr}$. From Fig. 6 it is clearly seen, that $\dot{q}_{cr}$ increases with the increasing roughness. For the roughest surface $\dot{q}_{cr}$ is about 60% higher than for the smooth surface and approaches the value estimated from equation (8) for stationary conditions. Specimens with low surface roughness tend to premature transition to film boiling.

The effect of transient conditions on $\dot{q}_{cr}$ may be compared with the results obtained by Sinha *et al.* [7] in the case of a wire heater. The authors of this paper reported a premature transition to stable film boiling for power densities of about 5 W cm^{-2}, which was only about 40% of the value of their stationary experiments.

5.3. *Onset of nucleate boiling*

The onset of boiling (see e.g. dash in curve no. 3 in Fig. 4) was detected by different methods, which are described in the following. The reproducibility of the instance of onset of boiling was estimated by comparing the measurements of three warming–cooling cycles for seven different power inputs. The scattering of the temperature of onset of boiling (ΔT_b) for a smooth specimen ($R_a < 0.1$ μm) was found to be about 0.8 K. This corresponds to a reproducibility of about 3% for ΔT_b and of about 6% for the time of onset of boiling (t_b).

The first possibility to determine the onset of boiling is to exploit the deviation from the $\Delta T \propto t^{1/2}$ behavior. This deviation can tend to lower or higher values of the excess temperature depending upon heat flux and surface roughness. The precision in the determination of the time of onset of boiling for a single curve is estimated to be about 3% for this method.

The second possibility to determine the onset of nucleate boiling was to record the intensity of the laser beam grazing the wetted surface. The sharp decrease in intensity can be correlated with the starting of bubble formation, as the liquid–vapour boundary of growing bubbles strongly attenuates the laser beam. Despite occasional perturbations of the laser-signal by particles (dust particles or ice particles) and slight liquid motion, its sharp decrease in most cases allows determination of the onset of bubble formation with an accuracy of about 2–3 ms.

The third method was to take a series of photographs during the heating. The instance, when bubble formation is explicitly observed over the heated region for the first time, is taken to be the time of onset of nucleate boiling. The uncertainty in time determination by photographs is given by the time between the flashes (typically about 5 ms).

As a first approximation the onset of boiling can be taken to be characterized by a constant excess temperature. This seems to be valid at least for rough surfaces (see Fig. 3). According to equation (2) a constant excess temperature ΔT_b at onset of boiling implies

$$t_b \cdot \dot{q}^2 = \text{const.}, \quad (9)$$

where t_b denotes the time at onset of boiling, and the constant depends upon the excess temperature ΔT_b and the thermal properties of the substrate and the coolant. Figure 7 compares results from the three methods to determine onset of boiling for a sample of roughness $R_a = 3.6$ μm. The results agree mostly within the errors stated. Exceptions are some laser-signals due to particle disturbances, which simulate bubble formation at shorter times. The agreement confirms the interpretation, that bubble nucleation takes place before convection can start. Otherwise bubble formation would not happen in coincidence with the deviation of the temperature from the $t^{1/2}$-behavior in the heat conduction regime. Furthermore, Fig. 7 shows the validity of equation (9) by comparison with a constant value for $t_b \cdot \dot{q}^2$ (see dotted line) from the laser experiment. Essential deviations are observed only for low values of $\dot{q}$, since the assumption (ΔT_b being independent of $\dot{q}$) is not fulfilled here.

The thermal signal was subsequently chosen for the determination of the onset of nucleate boiling. Figure 8 shows the surface temperature at onset of nucleate boiling (ΔT_b) as a function of $\dot{q}$. For large applied power inputs smooth surfaces have excess temperatures ΔT_b, which are about twice as large as for rough surfaces (see Fig. 8). This can be explained by the presence of active nucleation sites on rough surfaces, which arises by gas entrapment in grooves and cavities. These vapour bubbles preexist in relatively large numbers and sizes on rough surfaces and according to equation (4) need less superheating to be activated and to initiate nucleate boiling.

Furthermore, specimens of different roughness show a different dependence of excess temperature ΔT_b on $\dot{q}$. Where ΔT_b at rough surfaces tends to decrease and to approach a constant value, smoother

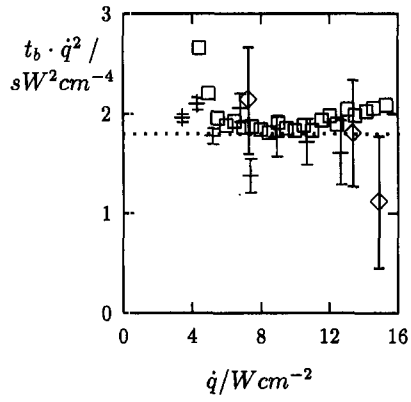

Fig. 7. Product from time at onset of nucleate boiling (t_b) and square of power density ($\dot{q}$) as a function of $\dot{q}$. Plotted values were determined by the deviation from the $\Delta T \propto t^{1/2}$ behavior (□), by breakdown in laser-signal (+) and by photographic observation (◇). A fit $t_b \cdot \dot{q}^2 = \text{const.}$ is also shown (···).

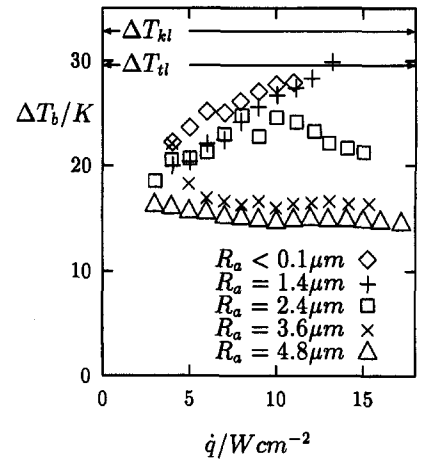

Fig. 8. Excess temperature ΔT_b at onset of nucleate boiling vs applied thermal power density ($\dot{q}$). The parameter is the mean surface roughness R_b.

surfaces show an increase in ΔT_b. In the case of very smooth surfaces with their lack of adequate nucleation sites the fundamental limits ΔT_{tl} and ΔT_{kl} become important. In our experiments this is observed in the case of high power input, when a $\Delta T \approx \Delta T_{tl}$ is reached within some milliseconds (see equation 2). The kinetic limit ΔT_{kl} might be reached by applying even higher power inputs which cause smaller rise-times, as demonstrated by Sinha *et al.* [24] for the wire-geometry.

5.4. *Vapor generation*

A series of photographs, partly shown in Fig. 9, gave information about the development of vapor generation in the transient process. They reveal the formation of many small bubbles all over the heated rough surface at the early stages of nucleate boiling (a). These simultaneously growing bubbles coalesce and form one big bubble, which grows by further vapor generation (b). The vapor-dome grows to a size that is much larger than bubbles which form and detach under stationary conditions. Finally, the large bubble becomes unstable and is divided into many smaller ascending bubbles. The size of the vapour-dome differs distinctly from the bubble departure diameter [18] of about 1 mm predicted for LN_2 in stationary experiments. This emphasizes the difference between transient and stationary processes as the onset of motion in the liquid as delayed in the former case (see also Sections 5.2 and 5.3).

The vapor volume can be correlated to the accumulated heat transferred to the liquid. Therefore photographs were used to determine the vapor volume. Visual interpretation allowed an accuracy of about 35%. To estimate the heat (Q_l) transferred to the liquid, numerical calculations were carried out. Therefore the one-dimensional equation of heat conduction was discretisized and solved explicitly. With the measured variation of the surface temperature as time-dependent boundary conditions, the heat flux ($\dot{q}_s$) into the

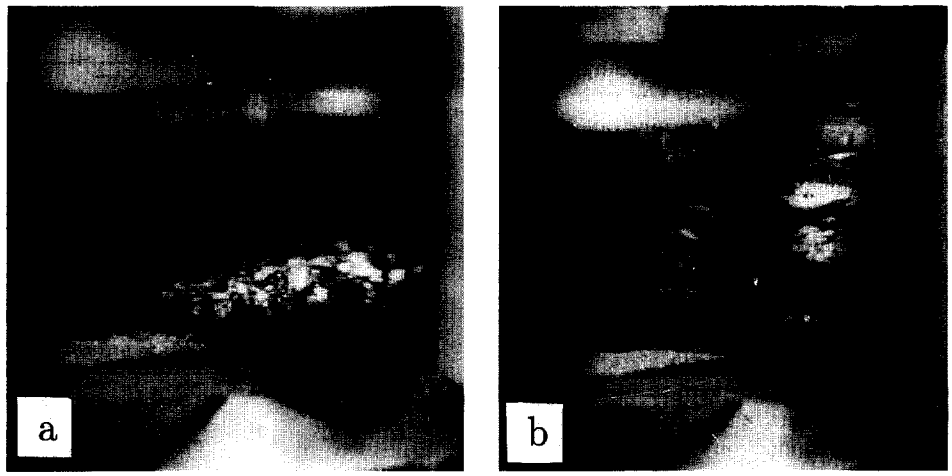

Fig. 9. Photographs taken (a) 18 ms and (b) 59 ms after initiation of the heat pulse. The sandblasted ($R_a = 4.8$ μm) specimen is heated by a mean power density of $\dot{q} = 14$ W cm^{-2}. The width of each picture corresponds to about 3.5 cm.

substrate was calculated numerically using Fourier's law. The total amount of heat transferred to the liquid was obtained by integrating $\dot{q} - \dot{q}_s$ over the time and considering the area of the heated surface.

Figure 10 shows the results obtained by photographs and numerical calculation in the described manner. The quantity Q_l per vapor volume V has to be compared with heat of vaporisation of nitrogen per volume gas. Within the error limit agreement was observed for the most of the measurement duration. Immediately after onset of nucleate boiling Q_l/V exhibits higher values, because of incomplete vaporisation of the superheated liquid. Obviously thermal and mechanical equilibrium is reached within some milliseconds and heat stored in the superheated liquid is rapidly transformed into generation of vapor. Thus vaporisation is the dominant mechanism of transient heat transfer after onset of nucleate boiling. This result

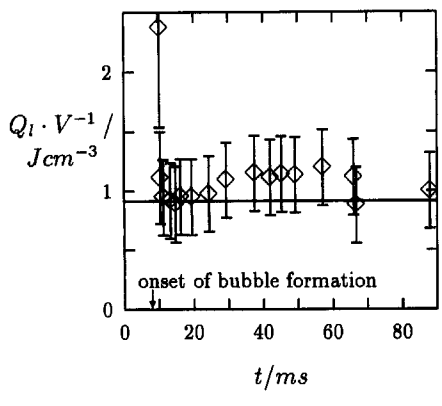

Fig. 10. Accumulated heat Q_l transferred to liquid per vapor volume V ($\diamond$) as a function of time. The data were obtained on the roughest specimen ($R_a = 4.8$ μm) heated with $\dot{q} = 14$ W cm^{-2}. For comparison the heat of vaporisation of LN_2 per volume of gas is also shown (——).

is consistent with the conclusion that convective effects are negligible on the examined time scale. Our findings may also be the base for a simplified theoretical model of transient heat transfer into coolants.

Acknowledgements—We would like to thank Professor Dr Harald Reiss (ABB, Heidelberg/Germany) and Dr Ove Nilsson (ZAE Würzburg) for helpful discussions and the company "Reinfurt Miniaturkugellager" (Rimpar/Germany) for the surface roughness measurements.

REFERENCES

1. T. Nakahara, Review of Japanese R&D on superconductivity, *Appl. Superconductivity* **1**, 177–189 (1993).
2. E. B. Forsyth, Superconducting power transmission systems—the past and possibly the future, *Supercond. Sci. Technol.* **6**, 699–714 (1993).
3. M. N. Wilson, *Superconducting Magnets*. Clarendon Press, Oxford (1983).
4. H. Reiss, An approach to the dynamic stability of high temperature superconductors, *High Temp.-High Press.* **25**, 135–159 (1993).
5. Patricia J. Giarratano and N. V. Frederick, Transient pool boiling of liquid helium using a temperature-controlled heater surface, *Adv. Cryogenic Engng* **25**, 455–465 (1980).
6. C. Schmidt, Transient heat transfer to liquid helium and temperature measurement with a response time in the microsecond region, *Appl. Phys. Lett.* **32**, 827–829 (1978).
7. D. N. Sinha, L. C. Brodie, J. S. Semura and F. M. Young, Premature transition to stable film boiling initiated by power transients in liquid nitrogen, *Cryogenics* **19**, 225–230 (1979).
8. A. Sakurai, M. Shiotsu and K. Hata, Boiling heat transfer characteristics for heat inputs with various increasing rates in liquid nitrogen, *Cryogenics* **32**, 421–429 (1992).
9. K. Okuyama and Y. Iida, Transient boiling heat transfer characteristics of nitrogen (bubble behaviour and heat transfer rate at stepwise heat generation), *Int. J. Heat Mass Transfer* **33**, 2065–2070 (1990).

10. E. Oker and H. Merte, A study of transient effects leading up to inception of nucleate boiling, *Heat Transfer* **1,** 139–144 (1978).
11. P. J. Giarratano, Transient boiling heat transfer from two different heat sources: small diameter wire and thin film flat surface on a quartz substrate, *In. J. Heat Mass Transfer* **27,** 1311–1318 (1984).
12. H. Rüthlein, Aufbau und Erprobung einer Apparatur zur Messung des Wärmeübergangs beim Blasensieden, Ph.D. Thesis, Universität Karlsruhe (1984).
13. R. D. Corty and A. S. Foust, Surface variables in nucleate boiling, *Chem. Engng Proc. Symp. Ser.* **17,** 51 (1955).
14. X. Zhou and K. Bier, Wärmeübergang an einem mit Oxidkeramik beschichteten Kupferrohr, DKV-Tagungsbericht 1993, Band II/1, 277–292, Deutscher Kälteund Klimatechnischer Verein e.V. (1993).
15. H. Schömann, A. Luke and D. Gorenflo, Size distributions of active nucleation sites with pool boiling heat transfer at single tubes with different roughness, *Heat Transfer* **5,** 63–68 (1994).
16. H. S. Carslaw and J. C. Jaeger, *Conduction of Heat in Solids* (2nd edn), p. 75. Clarendon Press, Oxford (1959).
17. M. Blander and J. L. Katz, Bubble nucleation in liquids, *A.I.Ch.E. Jl* **21,** 833–848 (1975).
18. V. P. Carey, *Liquid–Vapor Phase-Change Phenomena*, pp. 138, 181, 206 and 248. Hemisphere Publishing Corporation, Washington (1992).
19. J. E. Jensen, R. B. Stewart and W. A. Tuttle, *Selected Cryogenic Data Notebook*. Bubble Chamber Group, U.S. Atomic Energy Commission, New York (1968).
20. S. S. Kutadeladze, *Fundamentals of Heat Transfer*. Edward Arnold, London (1963).
21. Y. A. Kirichenko, S. M. Kozlov, K. V. Rusanov and E. G. Tyurina, Heat transfer crisis during liquid nitrogen cooling of high temperature superconductor, *Cryogenics* **31,** 979–984 (1993).
22. Y. S. Touloukian, R. W. Powell, C. Y. Ho, P. G. Klemens, *Thermophysical Properties of Matter, Vol. 2: Thermal Conductivity—nonmetallic solids*. IFI/Plenum, New York (1970).
23. N. P. Bansal, *Handbook of Glass Properties*. Academic Press, Orlando (1986).
24. D. N. Sinha, L. C. Brodie and J. S. Semura, Liquid-to-vapor homogeneous nucleation in liquid nitrogen, *Phys. Rev. B*, **36,** 4082–4085 (1987).